science, engineering and health studies

Research Article

Science, Engineering and Health Studies
https://li01.tci-thaijo.org/index.php/sehs
ISSN (Online): 2630-0087

Reforming time measurement of hydrophobic and hydrophilic insulator surface via centroid tracking

Poohthip Sonkaeo[1], Pished Bunnun[2], and Chanchai Techawatcharapaikul[1]*

[1] Department of Electrical Engineering, Faculty of Engineering, King Mongkut's University of Technology Thonburi, Bangkok 10140, Thailand
[2] National Electronics and Computer Technology Center, Pathum Thani 12120, Thailand

***Corresponding author**: Chanchai Techawatcharapaikul chanchai.tec@kmutt.ac.th*

***Received**: 16 August 2022*
***Revised**: 16 December 2022*
***Accepted**: 21 December 2022*
***Published**: 26 October 2023*

***Citation**: Sonkaeo, P., Bunnun, P., and Techawatcharapaikul, C. (2023). Reforming time measurement of hydrophobic and hydrophilic insulator surface via centroid tracking. Science, Engineering and Health Studies, 17, 23040003.*

ABSTRACT

Flashover between insulator surfaces is the most serious issue impacting power system stability related to power failures. It is caused by insulator surface degradation, which causes a flashover loss in insulation efficiency due to a change in the hydrophobicity class (HC) described in IEC TS 62073. The surface tension method is one of the measurement techniques used in this study. This study aimed to research an algorithm for transitioning from conventional measurement methods to a suggested approach for classifying surface tension based on the reforming time that applies to the centroid tracking technique. This research provides manual input for the automated image processing method. The main method is centroid tracking segmentation in a wet area (CTSWA). The comparative timing between adjacent manual frames was examined, yielding results known as ground truth (GT), and our approach (CTSWA) was demonstrated. Most results had a reforming time variance of less than 3% compared to GT. The use of the studied method yields three benefits, including automatic reforming time verification, which can produce acceptable results from more sensitive and reliable insulator inspections. It can also be applied to preventive maintenance planning (PM). Additionally, it reduces the limitations of human decision-making.

Keywords: image processing; centroid tracking; surface tension method; hydrophobic; hydrophilic; insulator

1. INTRODUCTION

Currently, electrical insulators are commonly used in power utilities. Cases using insulators in electrical systems include porcelain, polymers, and glass. The interaction of a strong electric field, air corrosion, ultraviolet radiation, pollution, rain damage, and porcelain insulator degradation by age can cause hydrophobicity. Not only does this waste the efficiency of electrical stability, but also reduces the performance of the flashover. A hydrophilic surface causes power system damage (Berg et al., 2001; Chen et al., 2005; Ramalla et al., 2015). Because of the aforementioned factors, this research is crucial.

The publication of the IEC TS 62073 standard established a measurement and verification standard. It included the contact angle method, the surface tension method, and the spray method for measuring hydrophobicity (IEC TS 62073, 2016). Two traditional laboratory methods, detecting contact angle and spray, have evolved with the development of advanced techniques for image processing. The static contact angle method was adopted from a model proposed by circle

and ellipse fitting algorithms (Xu, 2013). By utilizing the dynamic contact angle method and switching to the background subtraction method, the process was streamlined (Sonkaeo and Techawatcharapaikul, 2021a). The spray method is the subject of the most research in this field because it can be enhanced by applying classification techniques such as machine learning and neural network techniques (Sonkaeo and Techawatcharapaikul, 2021b). In this experiment, the surface tension technique was used to determine the method based on the surface time of the water droplet at rest changing in the reference surface area, called the reforming time. In conventional experiments, a timer is used to calculate the droplet reversal time when they are diffused over an insulating surface. However, this hypothesis utilizes image processing technology to reduce man-made errors, which contributes to applying the centroid tracking technique with a water droplet on the surface of an insulator to obtain data on reforming time. The intention is to conduct human verification on all acceptable artificial intelligence (AI) approaches.

The IEC TS 62073 standard serves as the basis for this study. The surface tension method is essential for determining hydrophobicity or hydrophilicity, which is necessary for validating the data on the water reforming time. However, human measurement of the time required for water reforming is limited by imprecise tolerances and performance. Initially, computer vision relied on motion analysis to determine the instantaneous movement of underlying physical points, pixel by pixel. The term for this is object tracking. Yilmaz et al. (2006) summarized the categories for various object shape-tracking tools. Object tracking is utilized in numerous scientific applications, such as real-time car video detection and tracking (Jazayeri et al., 2011), cell segmentation and tracking algorithms (Ulman et al., 2017), and the spatial relationship of human tracking on complex streaming video (Alabid, 2021), as well as some others. The structure of droplets is similar to cell tracking in image processing. Therefore, this research was based on concepts from a related field. Specifically, we were interested in objects tracked using the centroid tracking (CT) technique in Figure 1 to verify each frame between Figure 1 (a) and Figure 1 (b). Xing and Yang (2016) described techniques for cell detection and segmentation. In Ata et al. (2018), a green star based on centroid (GSBC) tracking white blood cells (WBC) algorithm was proposed by using blob analysis as opposed to the optical flow technique. This study used blob analysis to detect droplet water, as proposed by Ata. To ensure that the WBC monitoring process is maintained throughout the video, a simple predictor-based approach with two key factors, age and visibility count, is recommended (Meenatchi and Subhashini, 2014; Zhong et al., 2014). The return on investment (ROI) has aged since its debut, indicating that it has been observed. Therefore, the predictor describes the total number of frames in which the track was identified as visible, and the "age" expresses the number of frames that include the white cell during tracking from the time it was first identified (Barnich and Van Droogenbroeck, 2011). In addition, one factor contributes to the discrepancy: the alignment of cells (Rani and Priyadharsini, 2010). This WBC research can be adapted to measure the reforming time of the droplet's object using ROI.

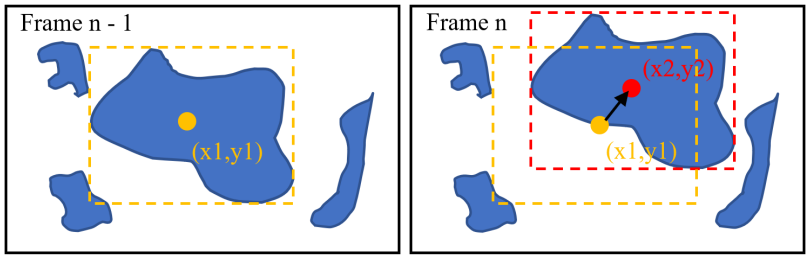

Figure 1. Object centroid tracking technique in each frame: (a) frame n – 1, (b) frame n

This research proposed utilizing the second method for measuring the hydrophobicity of insulator surfaces. This paper proposed a methodology for classifying porcelain insulators into hydrophobicity classes using the CT method. The centroid tracking segmentation in a wet area (CTSWA) would be compared to the standard methods of stopwatch manual (SW), which aimed to manually inspect adjacent frames, also known as the ground truth database (GT). Figure 2 illustrates the steps necessary to describe the concept of CT. The research key had the following objectives: 1) to investigate the properties of water surface tension that affect the time of change, 2) to research and develop a technique to precisely determine the timing of droplet reformation, 3) to differentiate between high and low surface tension characteristics using the IEC TS 62073 standard, and 4) to address the issue of human error in measuring.

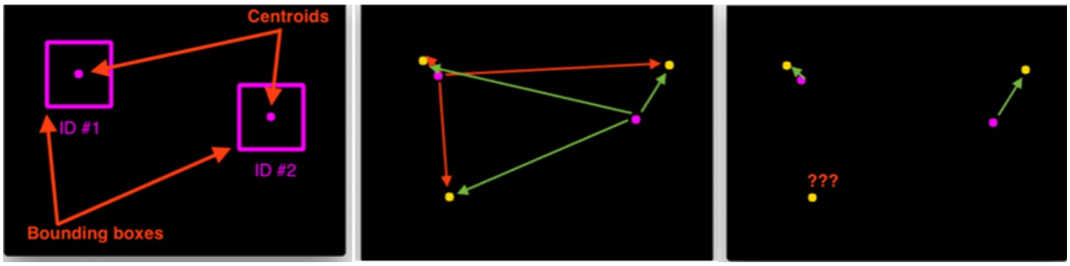

Figure 2. The first three steps of the centroid tracking concept: (a) frame a box around the centroid point; (b) compute the Euclidean distance between each centroid; (c) find the minimum distance between the pair of centroid points

2. MATERIALS AND METHODS

2.1 System overview

In this study, a digital camera with the Sony α7R with 36.4 MP sensor and a FE 50 mm f/1.8 lens, three sets of LED daylights (6500 K), a glass dropper lab, marker pens, cotton-tipped wooden applicators, a 50-mL graduated bottle containing distilled water, potassium permanganate ($KMnO_4$) at a maximum concentration of 0.03%, and a closed-loop environment-regulated laboratory in the department of Electrical Engineering in King Mongkut's University of Technology Thonburi (KMUTT), Thailand. That used to support the method.

2.2 Experiment design

Before conducting the experiments to simulate actual field circumstances in Figure 3, the following rules and procedures were adhered to:

Step 1: The experimental environment was adjusted to a controlled area with a temperature of 30 °C and a relative humidity of over 70%.

Step 2: Based on the hardware settings, the horizontal distance between the camera and the insulator sample should be Hx = 1–2 m. The ROI was then formed on the insulator surface sample by drawing a five-centimeter-wide frame with a marker pen (25 mm in diameter). Then, the reagent mixtures were provided. (To obtain a sample with a solution concentration in accordance with IEC TS 62073, a graduated bottle was filled with purified water and $KMnO_4$ added at a maximum concentration of 0.03%). Then, the insulator was positioned on a platform that could be adjusted to align the ROI with the focusing surface.

Step 3: After installing an insulator on the platform, a video was recorded as the third step. Then, using a glass dropper, three to four drops (three to four milliliters) of the reagent mixtures were applied to the surface of the insulator in the ROI area. After the reagents fell to the surface of the insulator, cotton-tipped wooden applicators were used to spread the reagent mixtures on the ROI area of the insulator surface and then immediately removed. The video recording was stopped once the water droplet stopped spreading.

Step 4: The preceding steps were repeated until a video of each sample has been created.

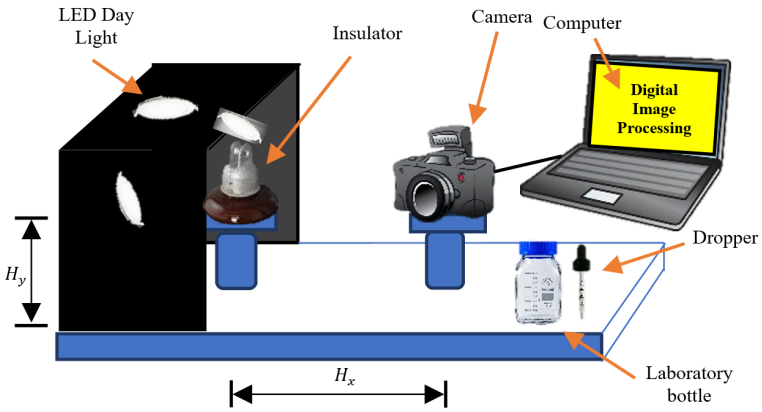

Figure 3. Illustration of equipments

Reforming time was used to determine whether a substance is hydrophilic or hydrophobic once all the videos from the experiment were collected. If the liquid keeps spreading for more than two seconds, a mixture should be considered to have a higher surface tension (hydrophilic). If the reforming water forms stationary droplets in less than two seconds, the mixture has a lower surface tension (hydrophobic). This research paper initiated and investigated the improvement of conventional method from manual measurement to computer vision applications in image processing. This research attempted to enhance an algorithm by demonstrating the effective results of the improved analysis method. Videos were transferred to a personal computer via USB using MATLAB v9.10 and Image Processing Toolbox v9.10, which are the primary software tools for creating an environment that is simple and user-friendly for image analysis.

2.3 Image processing procedure

Recognizing and localizing objects in images is one of the most crucial and difficult tasks for computer vision. In these experiments, more than 90 videos (1080 x 1920 x 3 uint8) were evaluated. The design of the block diagram is essential for determining the method's scope and anticipated outcomes. The authors began this research by designing and enhancing the algorithm on each block. Figure 4 shows the crucial steps following the transfer of experimental data as a video file into the image processing methods, which include A) Pre-processing, B) Detection of the cotton tip, C) Counting the frame of droplet reformation, and D) Conversion of the number of frames to time.

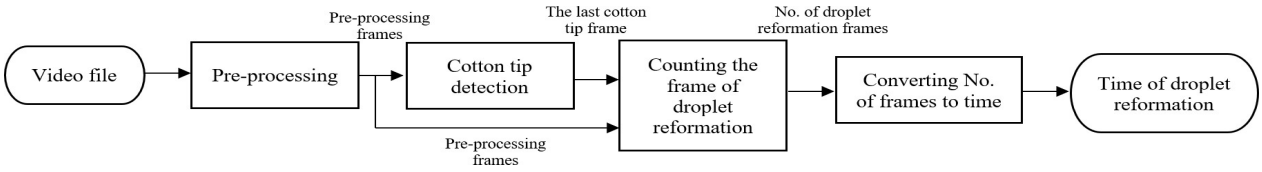

Figure 4. Block diagram of the proposed method

The output of this method was the time of droplet reformation, which displays the following information for each topic:

A. Pre-processing

Figure 5 shows a preliminary data processing procedure involving the importation of video files in (R, G, B) format into the capturing video frame input, which serves as a procedure for converting video data into frames. Furthermore, only the middle part of each collected image is placed in a rectangular region of 280 px x 230 px when cropping the ROI of the video.

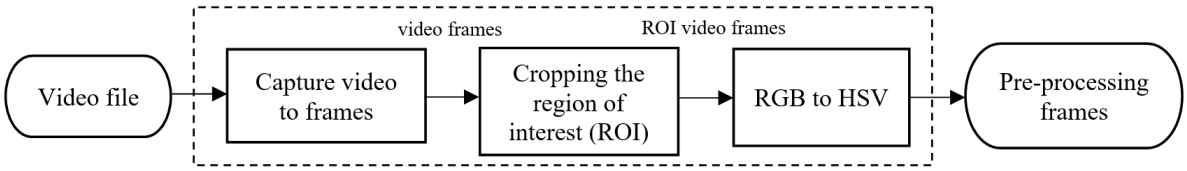

Figure 5. Block diagram of pre-processing step

The following step was used to track a cropped image to define the area of interest (ROI video frame) using the Bhattacharyya distance Equation (1 - 2), a color-based similarity metric (Trivedi and Mills, 2020).

$$C(I_T,I_R)=\int\sqrt{f_T(s)f_R(s)}ds \quad (1)$$

where,

$$D_B(I_T,I_R)=-\ln\left(BC(I_T,I_R)\right) \quad (2)$$

General edge detection cannot be split into the edge of the incoming droplet or the surface of the insulator. This is to avoid making a mistake when a mixture of reagents with the same color falls on the insulator surface. HSV color extraction can resolve this issue. The algorithm for pre-processing using RGB to HSV color space via image conversion (Hanumantharaju et al., 2012) is based on Equations (3-5). Using Equation (3) on the R, G, and B channels, the hue (H) element of the HSV color space can be discerned. This can be used as a parameter in the process of cotton tip detection.

$$H=\begin{cases}0+\frac{43\times|G-B|}{Max(R,G,B)-Min(R,G,B)}, if\ Max(R,G,B)=R\\ 85+\frac{43\times|B-R|}{Max(R,G,B)-Min(R,G,B)}, if\ Max(R,G,B)=G\\ 171+\frac{43\times|R-G|}{Max(R,G,B)-Min(R,G,B)}, if\ Max(R,G,B)=B\end{cases} \quad (3)$$

Where Max(R, G, B) is the maximum of the red, green, and blue pixels.

The saturation (S) element of the HSV color space can be derived from R, G, and B channels by Equation (4)

$$S=\left(\frac{Max(R,G,B)-Min(R,G,B)}{Max(R,G,B)}\right) \quad (4)$$

The value (V) component of HSV labelling color space is determined by Equation (5)

$$V=Max(R,G,B) \quad (5)$$

Figure 6 shows the four steps of the output in pre-processing frames, which are detailed in this section.

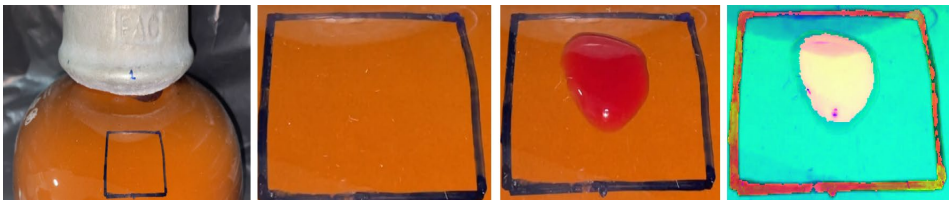

(a) (b) (c) (d)

Figure 6. Pre-processing stage result: (a) video frames, (b) ROI video frames, (c) droplet water on the insulator surface, and (d) pre-processing frames

B. Cotton tip detection

The block diagram of cotton tip detection is shown in Figure 7, after receiving pre-processing frames as HSV parameters input, which creates parameters for spreading cotton-tipped wooden applicators. The results of the cotton-tip detected frame involve a two-step process: detection and tracking.

B.1 Detection

Object detection aimed to eliminate pixels that did not have the same color as the object model. This part consisted of two steps:

a) Histogram projection

The first step refers to Hidayatullah and Konik (2011). We modified the method of separating each HSV image elements into hue image, saturation image, and value image, then formed the histogram projection in all of the images that generate the object modeling process shown in Figure 8.

The AND operator was used to combine these three histogram projection images into a single image. The input for the following process was the modified image.

b) Masking cotton-tip image

The next step was masking the cotton-tip image gained from HSV image conversion (pre-processing block) using the HSV projection step. This process could connect color-based and texture-based operations (Trivedi and Mills, 2020).

During this process, the value of each pixel in the HSV projection image was observed. The value of the pixel in the cotton-tipped picture with the same location as the examined pixel was changed to "0" if it was less than the threshold. However, pixels with a low probability of being an object's component were excluded if the threshold was changed to "255" in our target. The output of this step was the picture used as the input for the tracking step.

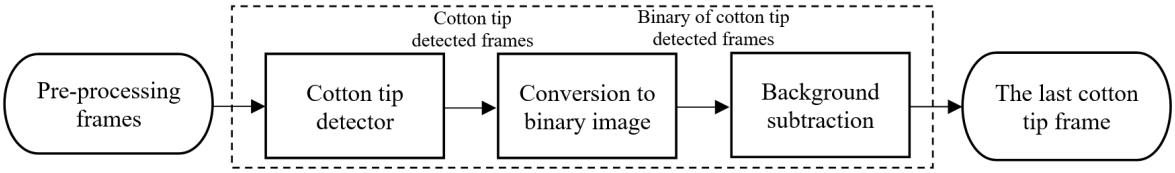

Figure 7. Block diagram of the cotton tip detection step

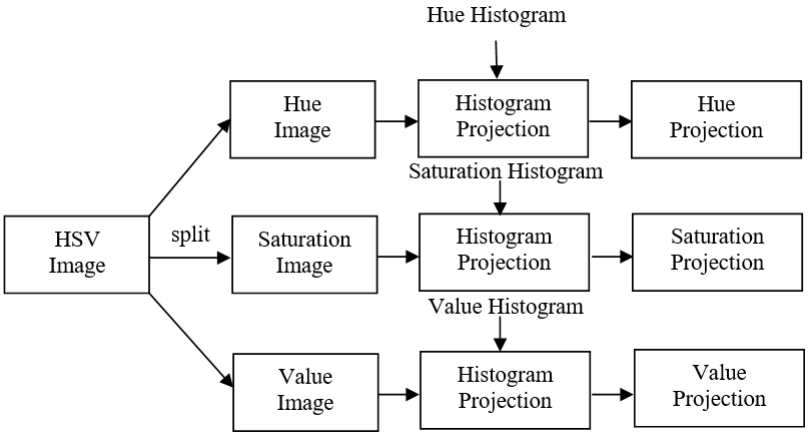

Figure 8. Generate object modeling by HSV histogram projection

B.2 Tracking

This step focused on texture matching between the cotton tip and the texture of the boundary object. The suggested concept used a predefined threshold value and the single largest component from the selected binarised image (0, 1). These were all performed through the cotton-tip segmentation (CS) process. Then, using the previous frame to contrast with the next frame, which would create CS, use equation (4) as follows:

$$CS(I_T, I_R) = \int \sqrt{f_T(s) f_R(s)} ds \qquad (6)$$

where,

$$|I(x, y, t) - I(x, y, t-1)| > Threshold \qquad (7)$$

In addition, from equation (7), (x, y, t) is an image at time t, and $(x, y, t-1)$ is the background at time t. The cotton-tipped wooden applicators were detected in ROI from double to logical values in a binary frame. The state of the cotton bud that fell out of the water droplets, as shown in Table 1, was the key algorithm to decide when considering the start of the timer.

In order to determine the reforming time of the stationary water droplet, the camera was set to capture a side view of the scene following the steps shown in Figure 9.

Table 1. Pseudo code for cotton tip detector process

Algorithm: Cotton tip detector process	
Input:	Pre_processing_frames
Output:	Cotton_tip frames

```
Initialize the Pre_processing_frames extract to H, S, V
Set i, j = True
[Row_size, Col_size] = Find_size(H)
Define Cotton_tip_frames(Row_size, Column_size)
  For i ≠ Row_size
    For j ≠ Col_size
      If [H,S,V](i,j) located in range of threshold
          Cotton_tip_frames(i,j) = True
      Else
          Cotton_tip_frames(i,j) = False
      End If
    End For
  End For
  Return Cotton_tip_frame
```

(a) (b) (c)

Figure 9. Cotton tip detection stage result: (a) cotton tip detected frames (HSV color), (b) cotton tip detected frames (detection stage), and (c) the last cotton tip frame (tracking stage)

C. Counting the frame of droplet reformation

The next block counted the number of frames captured during water droplet reformation detection is shown in Figure 10. The following algorithm took two inputs: the pre-processing frame and the last of the cotton tip frames. The results of counting the frame of droplet reformation consisted of four steps: ROI of wet area, component labeling, centroid point calculation, and centroid point differentiation.

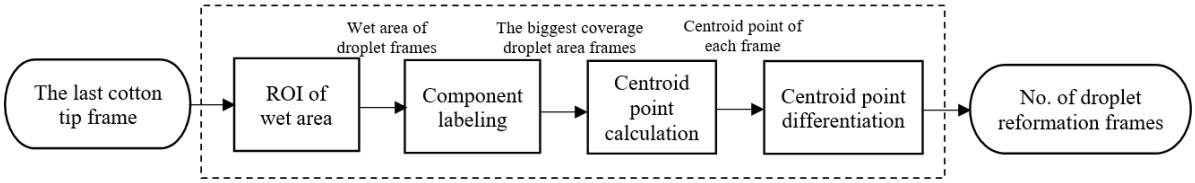

Figure 10. Block diagram of counting the frame of droplet reformation step

C.1 ROI of wet area

This step would start after passing through the last cotton tip frame. Droplet detection has a concept similar to the detection of a cotton tip, but uses another algorithm, HSV histogram color contrast (HCC) (Arulmurugan and Anadakumar, 2018). The aim was to prevent the cotton tip from absorbing some of the water onto the cotton, which would cause the color from the solution to adhere. The step was done by obtaining only the part of the salient value of a pixel edge of a droplet 'I_e' in image 'I' is given below:

$$alient(I_e) = \sum_{I_e, I_f \in I} Dis(I_e, I_f) \quad (8)$$

$$Salient(I_e) = Dis(I_e, I_1) + Dis(I_e, I_2) + \ldots + Dis(I_e, I_n) \quad (9)$$

From Equation (8), $Dis(I_e, I_f)$ represents the color distance between pixels. The objective of the HCC model was to integrate color uniqueness into identifying salient points, where vectors with equal information had an equal influence on the salient values. The salient value for each color was obtained by recreating Equation (9) so that equivalent color values were linked together. The salient value of the edge of the wet area was then converted to a binary image.

C.2 Component labeling

After detecting the droplet edge, a dilation of the ROI wet area step output was performed. Assume that A is the edge of the wet area in the resulting image and B is the structuring element (Cucchiara et al., 2003). Morphological close operation by dilation would be performed in Equations (10–11) as follows:

$$A \oplus B = \left\{ Z \middle| \left(\hat{B}\right) z \cap A \neq \emptyset \right\} \quad (10)$$

The following step determined where to fill the hole in the dilated image:

$$X_k = (X_{k-1} \oplus B) \cap A^c \quad (11)$$

After filling the hole in the dilated image, the objects also had some noise or small objects that we did not consider. The last step was to confine the required region that contained the biggest droplet on the insulator surface by removing the small objects that had fewer pixels than the biggest droplet from the binary frame. The method for defining the irregularity index of cells for droplet image segmentation is in Equation (12):

$$I = \frac{{D_c}^2}{A} \quad (12)$$

where I is an image, Dc is the perimeter of the droplet contour, and A is the area of the droplet on the insulator surface.

C.3 Centroid point calculation

The last binary images were received after the complete segmentation of the image. The droplet is $C_f^n = (X_f^n, Y_f^n)$, which means the n^{th} in frame f, and (X_f^n, Y_f^n) are the coordinates of distance from the centre point of the droplet (Centroid) in the image. Based on the premise that droplet mass was distributed equally, we computed the droplet centre with the centre of mass. The centroid calculation formula is described in Equation (13) below:

$$X_f = \frac{\sum X_n}{A};\ Y_f = \frac{\sum Y_n}{A}; \quad (13)$$

where X_f and Y_f are the coordinates of each pixel in the droplet, X_n and Y_n are the coordinates of the centroid, and A is the area of the biggest droplet in the binary image.

C.4 Centroid point differentiation

The last step in this block was finding the distance differences between the droplets in adjacent frames. Droplet assignment was frequently based on similarity with the study of Zhi et al. (2018), which used feature vectors, where the feature components include the droplet area, shape, intensity, and more. These cells and droplets of water had

some similar patterns, but the dynamic feature significantly changed their shape and size. To create a more general tracking method, only the droplet location was used, which is the most basic information and has nothing to do with droplet morphology. The challenge could then be considered particle tracking, but it was more complicated because different droplet behaviors, such as misshapen droplets, would result in particle changes. To improve the reliability of tracking, we presented an algorithm that, after calculating the centre stop time in each perfectly overlapped frame, could generate the point differentiation of the biggest droplet area. The following formula was used to determine the distance of a droplet; it could also compute the centroid in two separate frames along the x- and y-axes, and it can calculate the Euclidean distance using the given Equation (14):

$$D_{Centroid} = \sqrt{[X_f(i) - X_f(i-1)]^2 + [Y_f(i) - Y_f(i-1)]^2} \quad (14)$$

where $D_{Centroid}$ is the distance between adjacent frames, i is the number of frames and X_f and Y_f are the coordinates for each pixel in the droplet. The number of droplet reformation frames would be determined using the method shown in Figure 11. Figure 11 (b) is simple CL segmentation, while Figure 11 (c) is CTSWA after filling a hole in each wet area. The algorithm in this step is shown in Table 2 in detail below:

Table 2. Pseudo code for centroid point differentiation process

Algorithm: Centroid point differentiation process

Input: Centroid_point_each_frames, Video_frames
Output: No_of_droplet_reformation_frames

```
Initialize separate centroid axis by X_centroid, Y_centroid from Centroid_point_each_frames
[Row_time, Col_time] = Find_size(Video_frames)
Define Num_frames(Row_time, Col_time)
  For Row_time = True
    For i = 1: Col_time - 1
      Num_frames(i) = |Video_frames(i)-Video_frames(i+1)|
    End For
  End For
  Return Num_frames*
[Value_max, Position_max] = max(Num_frames)
//End of finding the maximum number of frames in each video
[Row_centroid, Col_centroid] = Find_size(Centroid_point_each_frames)
Define Diff_centroid (Row_centroid, Col_centroid)
  For Row_centroid = True
    For j = 1: Col_centroid – 1
      Diff_centroid(j) = |X_centroid(j) - X_centroid(j+ 1)| & |Y_centroid(j) – Y_centroid(j+ 1)|
    End For
  End For
  Return Diff_centroid *
//End of finding the difference distance of centroid point in each frame
[Row, Time_min] = min(Diff_centroid)
No_of_droplet_reformation_frames = Time_min
```

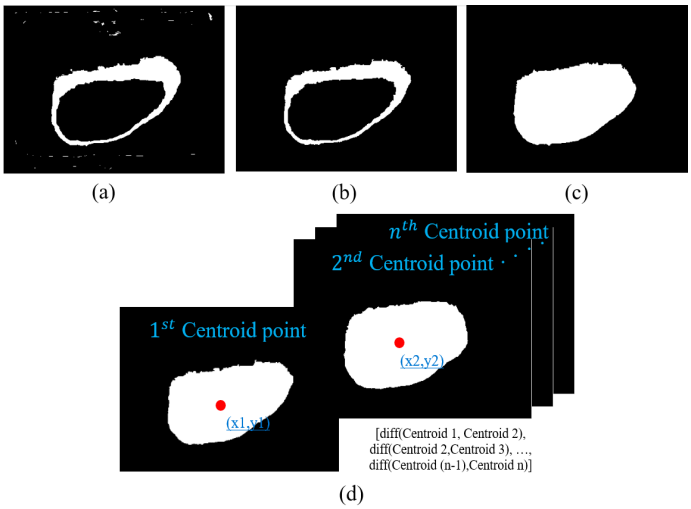

Figure 11. Counting the frame of droplet reformation stage result: (a) the wet area of droplet frames, (b) the process of CL, (c) the biggest coverage droplet area frames, and (d) the CT subtraction technique

D. Converting No. of frames to time

In Figure 12, the droplet reforming time was calculated by entering the number of droplet reformation frames and the frames per second (fps) into the convert frames to time process to create Equations (8) to convert results into seconds, which would result in the droplet deformation time that could be calculated using the following expression:

$$Time\ (s) = \frac{No.\ of\ droplet\ refomation\ frames}{fps} \quad (15)$$

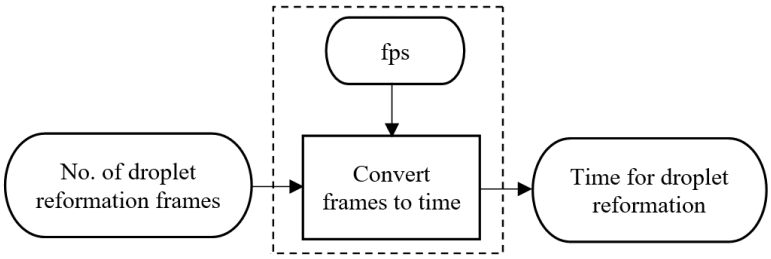

Figure 12. Block diagram of converting no. of frames to time

3. RESULTS AND DISCUSSION

3.1 Experiment results

The proposed algorithms (CTSWA) were derived from centroid tracking recognition, while spreading droplets could also be detected by droplet tracking on the insulator surface. To illustrate the correct detection and tracking of a droplet on the insulator surface, four main steps from Figure 7 were used. Every frame would be cropped from the ROI, leaving only 241 px x 354 px for computing faster and defining only the area of interest. The key contributions of CTSWA methods were 4 steps. First, converted RGB to HSV color space in order to detect the different color gradients by using the CS to track the cotton tip in the frame that was the condition for detecting the Hue thresholds = [0,1], Saturation thresholds = [0,0.04], and Value threshold = [0.95,1]. Afterward, it was converted to a binary image and created the condition area of the cotton-tip; if the area of the cotton tip was more than 500 px, it was concluded that cotton tips appeared in the frame. However, if the area of cotton tips was less than 50 px, it was concluded that cotton tips disappeared in the frame. Second, HCC was used to detect the unique edge of a droplet by using histogram thresholding for detecting the edge of a wet area, such as the Hue thresholds = [0.04, 0.06], Saturation thresholds = [0.7, 1], and Value threshold = [0.61, 0.9]. Third, the centroid point tracking and segmentation were the highlights of the proposed method; tracking would start after the cotton tip disappeared. Figure 13 shows the results of the timestamp for the video sample. The 237th frame to the 489th frame represented the state of using a dropper to drop the droplet on the insulator surface, while the 717th frame to the 765th frame represented the cotton tip spreading the droplet on the insulator surface, and the 766th frame to the 865th frame represented the droplet reforming. The state of the centroid point calculation would launch from the HCC of the wet area and stop while the different points of the centroid were at zero. The last step was converting the number of frames to time in the second unit. Thus, the results of this experiment are shown in Figure 14.

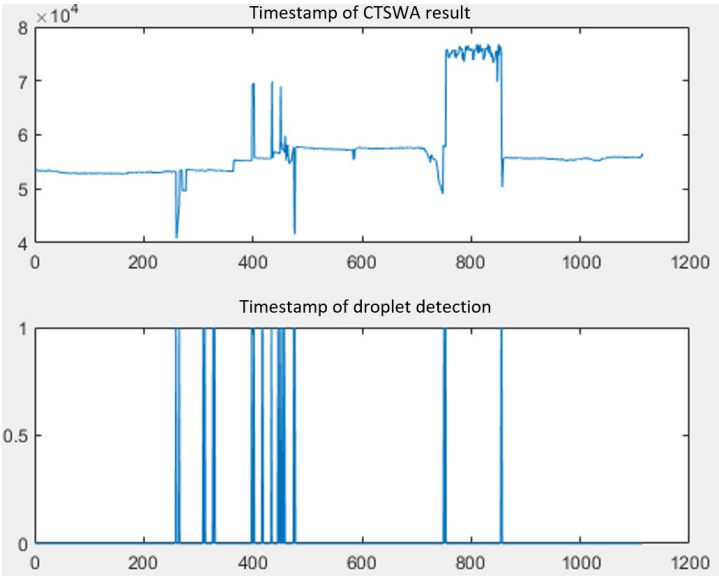

Figure 13. Timestamp of CTWA method

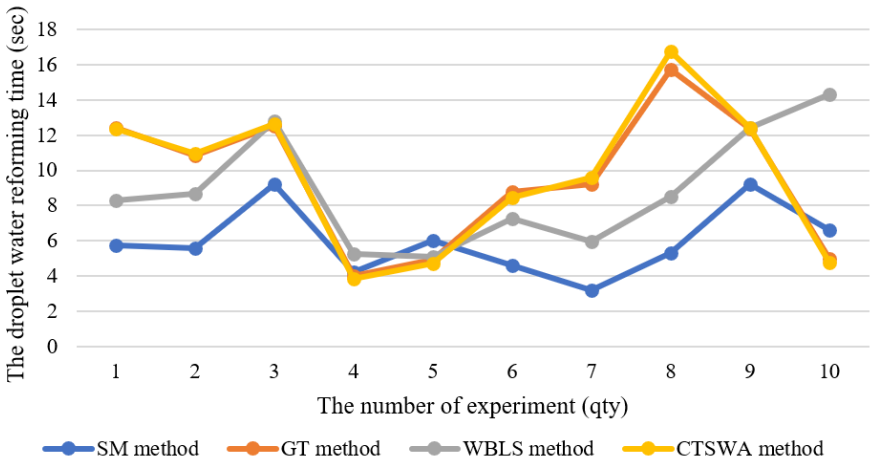

(a) Insulation no.1

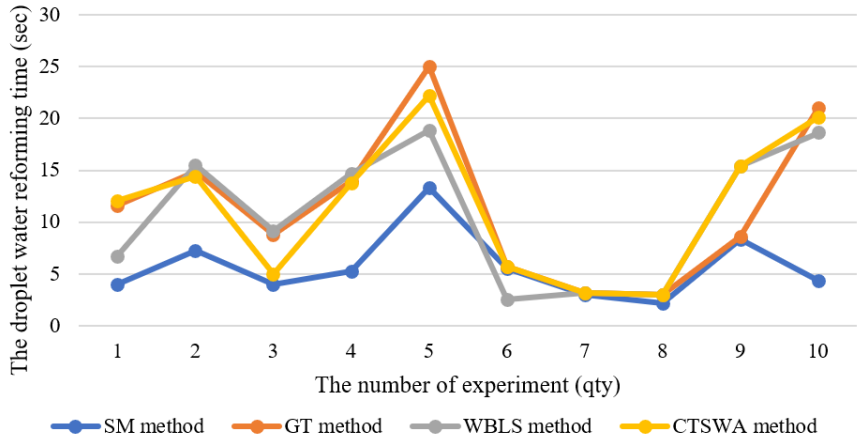

(b) Insulation no.2

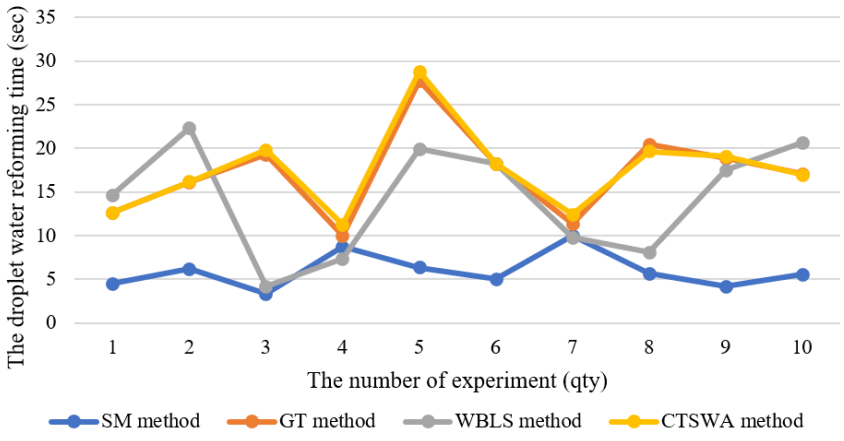

(c) Insulation no.3

Figure 14. The relationship between the water droplet reforming time and the number of experiments of insulators (a)-(c)

3.2 Benchmark results

Table 3. Training the result of each method

Training data	The average droplet reforming time (s)				The percentage of difference reforming time (%)		
	GT	*SW*	*WBLS*	*CTSWA*	*GT-SW*	*GT-WBLS*	*GT-CTSWA*
1st insulator 1st side	9.581	5.967	8.866	9.652	37.721	7.463	0.7410
1st insulator 2nd side	13.713	4.651	11.954	13.293	66.083	12.827	3.063
1st insulator 3rd side	15.129	10.489	15.569	14.049	30.670	2.908	7.138
2nd insulator 1st side	11.581	5.728	10.771	11.498	50.540	0.717	0.716
2nd insulator 2nd side	12.406	7.133	14.417	12.624	42.504	16.210	1.757
2nd insulator 3rd side	14.836	9.611	15.248	14.598	35.218	2.702	1.604
3rd insulator 1st side	17.179	5.943	14.283	17.522	65.405	16.858	1.996
3rd insulator 2nd side	16.424	6.717	16.126	16.322	59.103	1.8144	0.102
3rd insulator 3rd side	12.913	8.649	12.569	12.623	33.021	2.664	2.246

Table 4. Accuracy result of each method

Method	Accuracy (%)
SW	53.304
WBLS	92.871
CTSWA	97.849

Table 3 compared the accuracy of datasets for each method, such as the average droplet reforming time and the percentage of difference reforming time. Evaluating the proposed method (CTWA) in comparison with the traditional methods from GT and SW was achieved by humans, and WBLS with a background subtraction technique (Xing and Yang, 2016) from another technique of detection in training benchmark datasets. More than 90 videos of reforming droplet porcelain insulators were used in this research. There were three samples of insulators; all 3 sides were tested in 10 videos per side. To reduce the reforming time error from the results, the mean of each side of the insulator was used from all ten videos for training data with the same pixel scale. From the average droplet reforming time, all samples had a reforming time greater than 2 s, which could indicate that the mixture had high surface tension (hydrophilic) according to the conditions of the surface tension method to IEC TS 62073. The percentage difference in reforming time when compared with GT what we referred to as the standard to verify with another method. Figure 15 shows a grouped frequency distribution from 90 sample videos of each method. The height of distribution between GT (Blue color) and CTSWA (Purple color) was from 2 s. to 27 s., which comprised the closest datasets to the symmetric histogram, suggesting that the process for these methods was mostly stable and within the specified standards with slight variations. The results of the reforming time box plot are illustrated in Figure 16. The median of GT was 12.48 s., SW was 6.28 s., WBLS was 12.54 s., and CTSWA was 12.44 s. The range of GT had 24.66, SW had 20.92, WBLS had 24.02, and CTSWA had 25.29. The interquartile range (IQR) of GT had 8.18, SW had 4.36, WBLS had 10.31, and CTSWA had 8.87. Therefore, the median, range and IQR values closest to GT were CTSWA.

The percentage of difference in reforming time could be calculated using the following equations (16):

$$\% \, Diff \; = \left| \frac{(X_i - X_{GT})}{X_{GT}} \right| * 100 \qquad (16)$$

where $\% \, Diff$ is the percentage of difference reforming time, X_i is the measured value, and X_{GT} is the ground truth value. It represented the indicators from the above data that may be used to calculate the percentage difference from GT, yielding the following results: GT-SW was 46.696%, GT-CTSED was 7.129 %, and GT-CTSWA was 2.151%. Consequently, Table 4 could summarize the sequence from the lowest to highest accuracy, starting with SW, WBLS, and CTSWA, respectively.

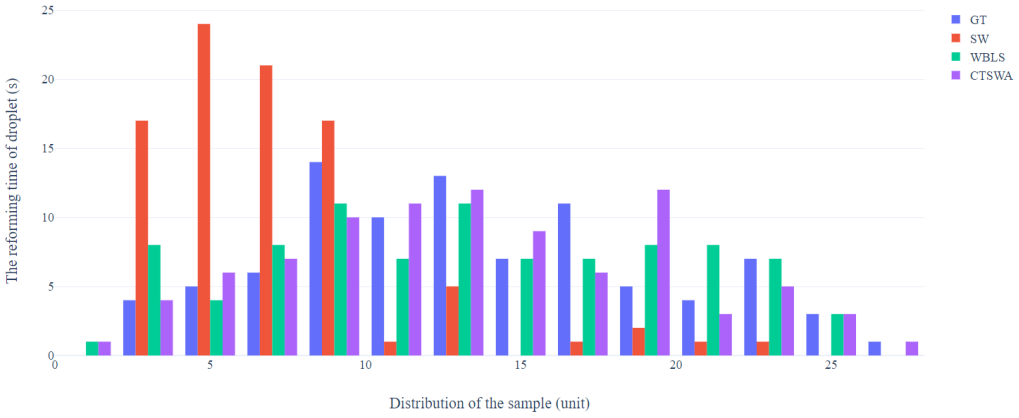

Figure 15. Histogram of the result of reforming time in each method

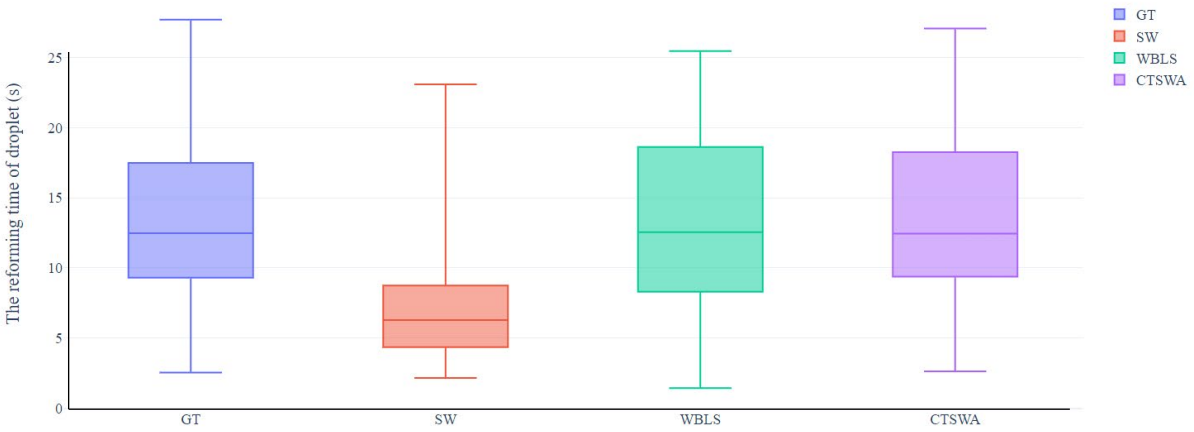

Figure 16. Box plot of the result of reforming time in each method

4. CONCLUSION

This study initiated and investigated the improvement of the traditional method of manual measurement to image processing applications. It attempted to investigate the technique to improve an algorithm by demonstrating the outcomes of an effective analysis technique. The application of an experiment employed the CTSWA image processing technology to determine whether each insulator was hydrophobic or hydrophilic. Using the surface tension method from IEC TS 62073, the performance of the insulator surface of the material was measured and evaluated to ensure conformance with the standard. It could be concluded that the proposed method is a useful classification tool for distribution network operators to distinguish between high (hydrophilic) surface tension and low surface tension (hydrophobic). It can provide automatic reforming time verification, be applied to preventive maintenance planning (PM), and minimize the limitations of human decision-making.

ACKNOWLEDGMENT

This work is supported by the "Thailand Graduate Institute of Science and Technology (TGIST)" funded under "National Science and Technology Development Agency (NSTDA)" CA-CO-2564-14614-TH, Thailand, and by the King Mongkut's University of Technology Thonburi (KMUTT) research fund.

REFERENCES

Alabid, N. (2021). Interpretation of spatial relationships by objects tracking in a complex streaming video. *ECTI Transactions on Computer and Information Technology*, 15(2), 245–257.

Arulmurugan, R., and Anadakumar, H. (2018). Region-based seed point cell segmentation and detection for biomedical image analysis. *International Journal of Biomedical Engineering and Technology*, 27(4), 273–289.

Ata, M. M., Ashour, A. S., Guo, Y., and Abd Elnaby, M. M. (2018). Centroid tracking and velocity measurement of white blood cell in video. *Health Information Science and Systems*, 6, 20.

Barnich, O., and Van Droogenbroeck, M. (2011). ViBe: A universal background subtraction algorithm for video sequences. *IEEE Transactions on Image Processing*, 20(6), 1709–1724.

Berg, M., Thottappillil, R., and Scuka, V. (2001). Hydrophobicity estimation of HV polymeric insulating materials development of a digital image processing method. *IEEE Transactions on Dielectrics and Electrical Insulation*, 8(6), 1098–1107.

Chen, X., Li, C., Huang, X., Zhao, L., and Song, W. (2005). On-line estimating the level of hydrophobicity of composite insulators using the digital images. In *Proceedings Electrical Insulation Conference and Electrical Manufacturing Expo*, pp. 216–221. Indianapolis, India.

Cucchiara, R., Grana, C., Piccardi, M., and Prati, A. (2003). Detecting moving objects, ghosts, and shadows in video streams. *IEEE Transactions on Pattern Analysis and Machine Intelligence*, 25(10), 1337–1342.

Hanumantharaju, M. C., Vishalakshi, G. R., Halvi, S., and Satish, S. B. (2012). A novel FPGA based reconfigurable architecture for image color space conversion. In *Global Trends in Information Systems and Software Applications. ObCom 2011. Communications in Computer and Information Science, vol 270* (Krishna, P. V., Babu, M. R., and Ariwa, E., Eds.), pp. 292–301. Berlin, Heidelberg: Springer.

Hidayatullah, P., and Konik, H. (2011). CAMSHIFT improvement on multi-hue object and multi-object tracking. In *Proceedings of the 2011 International Conference on Electrical Engineering and Informatics*, pp. 1–6. Bandung, Indonesia.

IEC TS 62073. (2016). *Guidance on the measurement of hydrophobicity of insulator surfaces*. [Online URL: https://standards.globalspec.com/std/9991614/iec-ts-62073] accessed on May 17, 2021.

Jazayeri, A., Cai, H., Zheng, J. Y., and Tuceryan, M. (2011). Vehicle detection and tracking in car video based on motion model. *IEEE Transactions on Intelligent Transportation Systems*, 12(2), 583–595.

Meenatchi, K., and Subhashini, P. (2014). Multiple object tracking and segmentation in video sequences. *International Journal of Advance Research in Computer Science and Management Studies*, 2(5), 71–79.

Ramalla, I., Gupta, R. K., and Bansal, K. (2015). Effect on superhydrophobic surfaces on electrical porcelain insulator improved technique at polluted areas for longer life and reliability. *International Journal of Engineering & Technology*, 4(4), 509–519.

Rani, T. J., and Priyadharsini, S. S. (2010). Region of interest tracking in video sequences. *International Journal of Computer Applications*, 3(7), 32–36.

Sonkaeo, P., and Techawatcharapaikul, C. (2021a). Hydrophobicity class of porcelain insulators based on information image feature extraction via image processing. *International Journal of Industrial Electronics and Electrical Engineering*, 9(1), 12–15.

Sonkaeo, P., and Techawatcharapaikul, C. (2021b). The hydrophobicity class of porcelain insulator detection based on digital image processing: A paper review. In *Proceedings of the 18th International Conference on Electrical Engineering/Electronics, Computer, Telecommunications and Information Technology*. pp. 759–762. Chiang Mai, Thailand.

Trivedi, M. M., and Mills, J. K. (2020). Centroid calculation of the blastomere from 3D Z-Stack image data of a 2-cell mouse embryo. *Biomedical Signal Processing and Control*, 57(4), 101726.

Ulman, V., Maška, M., Magnusson, K. E. G., Ronneberger, O., Haubold, C., Harder, N., Matula, P., Matula, P., Svoboda, D., Radojevic, M., Smal, I., Rohr, K., Jaldén, J., Blau, H. M., Dzyubachyk, O., Lelieveldt, B., Xiao, P., Li, Y., Cho, Y., … Ortiz-de-Solorzano, C. (2017). An objective comparison of cell-tracking algorithms. *Nature Methods*, 14, 1141–1152.

Xing, F., and Yang, L. (2016). Robust nucleus/cell detection and segmentation in digital pathology and microscopy images: A comprehensive review. *IEEE Reviews in Biomedical Engineering*, 9, 234–263.

Xu, Z. (2013). A static contact angle algorithm for silicone rubber aging experiments. *IEEE Transactions on Power Delivery*, 28(1), 491–498.

Yilmaz, A., Javed, O., and Shah, M. (2006). Object tracking: A survey. *ACM Computing Surveys*, 38(4), 13.

Zhi, X., Meng, S., and Shen, H. (2018). High density cell tracking with accurate centroid detections and active area-based tracklet clustering. *Neurocomputing*, 295, 86–97.

Zhong, Q., Chen, Z., Zhang, X., and Hu, G., (2014). Feature-based object location of IC pins by using fast run length encoding BLOB analysis. *IEEE Transactions on Components, Packaging and Manufacturing Technology*, 4(11), 1887–1898.